

## EVOLUTION OF THE RELATIVISTIC PLASMOID-CHAIN IN THE POYNTING-DOMINATED PLASMA

MAKOTO TAKAMOTO

Max-Planck-Institut für Kernphysik, Heidelberg, Germany  
Draft version July 23, 2013

### ABSTRACT

In this paper, we investigate the evolution of the plasmoid-chain in a Poynting-dominated plasma. We model the relativistic current sheet with cold background plasma using the relativistic resistive magnetohydrodynamic approximation, and solve its temporal evolution numerically. We perform various calculations using different magnetization parameters of the background plasma and different Lundquist numbers. Numerical results show that the initially induced plasmoid triggers a secondary tearing instability, which gradually fills the current sheet with plasmoids, as has also been observed in the non-relativistic case. We find the plasmoid-chain greatly enhances the reconnection rate, which becomes independent of the Lundquist number, when this exceeds a critical value. In addition, we show the distribution of plasmoid size becomes a power law. Since magnetic reconnection is expected to play an important role in various high energy astrophysical phenomena, our results can be used for explaining the physical mechanism of them.

*Subject headings:* magnetic fields, magnetohydrodynamics (MHD), relativistic processes, plasmas

### 1. INTRODUCTION

Magnetic reconnection is a process that converts magnetic field energy into thermal and kinetic energy very efficiently (Biskamp 2000; Priest & Forbes 2000). Because of this, it is believed that magnetic reconnection plays an important role in various phenomena from the laboratory plasma to the astrophysical plasma. Recently, interest in the properties of relativistic magnetic reconnection has been growing, especially in Poynting-dominated plasmas, which are believed to be present in various high energy astrophysical phenomena, such as ultra relativistic jets (Lovelace & Romanova 2003; Barkov & Baushev 2011), gamma ray bursts (GRB) (Lyutikov & Blandford 2003; Zhang & Yan 2011), and pulsar winds (Kennel & Coroniti 1984a,b; Lyubarsky & Kirk 2001; Kirk & Skjæraasen 2003). In those models, the Poynting energy of the plasma is assumed to be dissipated into thermal and kinetic energy almost completely at some distance from the central object. However, such an efficient dissipation process is still unknown. In the last decade, several studies have been performed with the goal of finding efficient dissipation processes (Lazarian & Vishniac 1999; Komissarov et al. 2007b; Takamoto et al. 2012; Inoue 2012; Amano & Kirk 2013; Mochol & Kirk 2013a,b). Magnetic reconnection is one of the most promising candidates among them, and has been studied actively from analytical (Blackman & Field 1994; Lyutikov & Uzdensky 2003; Lyubarsky 2005) and numerical points of view (Komissarov et al. 2007a; Zenitani et al. 2009b,a; Dumbser & Zanotti 2009; Zenitani et al. 2010; Takahashi et al. 2011; Bessho & Bhattacharjee 2012).

For magnetic reconnection to be occurred, the plasma should contain current sheets. Such structures evolve into the Sweet-Parker configuration when the Lundquist number  $S_L \equiv c_A L / \eta$  is small (Loureiro et al. 2005), where  $c_A$  is the Alfvén velocity,  $L$  is the sheet length,  $\eta$  is the resistivity. It is well-known that the reconnection rate of the Sweet-Parker sheet is very slow (Sweet 1958; Parker 1957, 1963), so that a considerable number of studies have been conducted on finding an enhancement mechanism of the magnetic re-

connection, such as the anomalous resistivity in the collisionless plasma (Ugai & Zheng 2005; Fujimoto 2011) and the turbulent effect (Lazarian & Vishniac 1999; Kowal et al. 2009). Recently, it was found that spontaneous current sheet fragmentation in a non-relativistic plasma occurs via secondary tearing instabilities when the Lundquist number exceeds a critical value, leading to the so-called plasmoid-chain. The critical value is thought to be about  $10^4$  in the non-relativistic plasma (Shibata & Tanuma 2001; Loureiro et al. 2007; Samtaney et al. 2009; Uzdensky et al. 2010; Bárta et al. 2011b; Loureiro et al. 2012; Huang & Bhattacharjee 2013; Loureiro et al. 2013). In those works, it was shown that (1) the reconnection rate is enhanced by the plasmoid-chain and reaches typically  $v_R \sim 10^{-2} c_A$ ; (2) the distribution of plasmoid size is either power law  $w^{-p}$  or an exponential function  $\exp[-w/\alpha']$  where  $p$  is the power law index,  $w$  is the plasmoid width, and  $\alpha'$  is a constant. Since the plasma temperature in the plasmoid region is higher than that of background plasmas, the plasmoid-chain is expected to generate pulsed emissions. Hence, the plasmoid-chain is of interest from observational and theoretical points of view, especially in connection with the solar flare (Bárta et al. 2011a).

The first study of relativistic plasmoid-chain was given by Zanotti & Dumbser (2011). They performed 2-dimensional and 3-dimensional numerical simulations of the relativistic magnetic reconnection using the relativistic resistive magnetohydrodynamic approximation (Dumbser & Zanotti 2009). In those calculations, they assumed a background plasma with high Lundquist number  $S_L \sim 10^5 - 10^8$ , relativistic temperature  $k_B T \sim mc^2$  and high magnetization parameter with respect to the mass density:  $\sigma_m \equiv B_0^2 / 4\pi\rho_0\gamma_0^2 \sim 20$  where  $B_0, \rho_0, \gamma_0$  are the background magnetic field in the laboratory frame, rest mass density and Lorentz factor, respectively. They also assumed the existence of a local anomalously large resistivity, so that their current sheet became very similar to the Petschek type one. They found that relativistic magnetic reconnection is similar to Petschek-type reconnection with a critical Lundquist number  $\sim 10^8$ , which is much larger than the non-relativistic cases.

In this paper, we investigate the evolution of the plasmoid-chain in a cold Poynting-dominated background plasma with

large Lundquist number:  $S_L \sim 10^3 - 10^5$ . In particular, we mainly investigate statistical properties of the plasmoid-chain, such as the distribution function of the plasmoid width and the dynamics of X and O-points along the current sheet. To study the evolution of the secondary tearing instability, we use a uniform, constant resistivity, and initialize the magnetic field with a perturbations localized at the origin. This enables us to understand the evolution of current sheets in which a tearing instability is triggered at a point.

## 2. FORMATION OF PLASMOID-CHAIN

In this section, we give a brief review of the non-relativistic plasmoid-chain theory.

It is widely known that current sheets are unstable to the tearing instability. The maximum growth rate of this instability can be expressed as:  $\omega_{max} = 1/\sqrt{\tau_R \tau_A}$  where  $\tau_R \equiv \delta^2/\eta$  is the resistive diffusion timescale and  $\tau_A \equiv \delta/c_A$  is the Alfvén crossing time across a current sheet,  $\delta$  is the sheet thickness,  $\eta$  is the resistivity, and  $c_A$  is the Alfvén velocity in the background plasma (Furth et al. 1963; Low 1973; Komissarov et al. 2007a). This expression can be rewritten as follows:

$$\omega_{max} = 1/\sqrt{\tau_R \tau_A} = \left( \frac{\delta}{c_A} \frac{\delta^2}{\eta} \right)^{-1/2} = \frac{\tau_A^{-1}}{\sqrt{S_\delta}}, \quad (1)$$

where  $S_\delta = c_A \delta/\eta$  is the Lundquist number related to the sheet thickness  $\delta$ . This equation shows the tearing instability grows faster as the sheet thickness  $\delta$  shrinks. The current sheet thickness behind plasmoids shrinks when the plasmoid grows along the current sheet, and this triggers the growth of other small plasmoids, which are called secondary plasmoids. Hence, we can expect that a current sheet would evolve into a stochastic plasmoid-chain in a few growth times of the largest plasmoid. Uzdensky et al. (2010) examined the existence of a critical Lundquist number  $S_c$  at which current sheets become unstable to the plasmoid instability, and discussed the physical nature of the plasmoid-chain. This critical value introduces the smallest elementary structure in the chain, called the ‘‘critical layer’’; the related key parameters are the length scale  $L_c = S_c \eta/c_A$ , the thickness  $\delta_c = L_c/\sqrt{S_c}$  and the reconnection rate  $v_R = c_A/\sqrt{S_c}$ . The authors also showed that the global reconnection rate is independent of the Lundquist number  $S_L$  when  $S_L > S_c$  and the plasmoid-chain reaches a statistical steady state. They obtained the global reconnection rate value as:  $v_R \sim 10^{-2} c_A$  by assuming the value of the critical Lundquist number to be  $S_c \sim 10^4$  in accordance with the results of their numerical simulations.

As is explained by Loureiro et al. (2007) and Bhattacharjee et al. (2009), the above expression of the growth rate of the tearing instability  $\omega_{max}$  can be reinterpreted as follows. When we consider the Sweet-Parker current sheet, we can obtain a relation between sheet thickness  $\delta$  and sheet length  $L$ :  $\delta \sim L/\sqrt{S_L}$  where  $S_L \equiv L c_A/\eta$ . Using this relation, the above equation can be rewritten as follows:

$$\omega_{max} \sim \frac{c_A}{L} \frac{L}{\delta} \sqrt{\frac{L}{\delta S_L}} \sim \frac{S_L^{1/4}}{\tau_{A,L}}, \quad (2)$$

where  $\tau_{A,L} = L/c_A$ . This equation means that the growth of the tearing instability becomes very fast when  $S_L$  reaches about  $10^4$ , which they considered as the critical value of the Lundquist number.  $S_L$  depends on the current sheet length  $L$  and this means we need a very large numerical domain to study the effect of the plasmoid-chain.

Name	$\sigma_{in}$	$c_A/c$	$S_L \times 10^{-5}$	$S_\delta$
B1	0.14	0.354	1.13	354
B2	1.4	0.767	2.45	767
B3	14	0.967	3.09	967
B4	29	0.983	3.14	983

TABLE 1

LIST OF SIMULATION PARAMETERS OF BASIC RUNS.  $\sigma_{in} \equiv B_0^2/4\pi\rho_0 h_0 \gamma_0^2$  IS THE MAGNETIZATION PARAMETER WHERE  $B_0, \rho_0, h_0, \gamma_0$  ARE THE UPSTREAM MAGNETIC FIELD, THE REST MASS DENSITY, THE SPECIFIC ENTHALPY, AND THE LORENTZ FACTOR, RESPECTIVELY;  $c_A$  IS THE ALFVÉN VELOCITY,  $S_L \equiv L c_A/\eta$  IS THE LUNDQUIST NUMBER RELATED TO THE SHEET LENGTH  $L$  AND  $S_\delta \equiv \delta c_A/\eta$  IS THE LUNDQUIST NUMBER RELATED TO THE SHEET THICKNESS  $\delta$ .

A more complete derivation is presented in (Bhattacharjee et al. 2009; Uzdensky et al. 2010; Loureiro et al. 2013).

## 3. NUMERICAL SETUP

We model a very long current sheet using the relativistic resistive magnetohydrodynamic approximation. We use the resistive relativistic magnetohydrodynamics (RRMHD) scheme developed by Takamoto & Inoue (2011) extended to the multi-dimensional case using the unsplit method (Gardiner & Stone 2005, 2008). To preserve the divergence free constraint on the magnetic field, we use the constrained transport algorithm (Evans & Hawley 1988). We calculate the RRMHD equations in a conservative fashion, and the mass density, momentum, and energy are also conserved within machine round-off error. For the equation of state, we assume a relativistic ideal gas with  $h = 1 + (\Gamma/(\Gamma - 1))(p/\rho)$  where  $\Gamma = 4/3$ ,  $h$  is the specific relativistic enthalpy,  $\rho$  is the rest mass density, and  $p$  is the gas pressure.

For our numerical calculations, we prepare a square domain,  $[0, L_x] \times [0, L_z] = [0, 20\delta] \times [0, 320\delta]$ , where  $\delta$  is the current sheet thickness. We divide it into homogeneous numerical meshes with size  $\Delta = 5\delta/128 \sim 0.04\delta$  which is equivalent to the mesh number  $N_x \times N_z = 512 \times 8192$ . Note that to reduce computational costs we solve only a quarter region of the current sheet and impose the point symmetric boundary condition about  $(x, z) = (0, 0)$  following Zenitani et al. (2009a). Hence, the above set up is equivalent to a square domain,  $[-L_x, L_x] \times [-L_z, L_z] = [-20\delta, 20\delta] \times [-320\delta, 320\delta]$  divided by the mesh number  $N_x \times N_z = 1024 \times 16384$ <sup>1</sup>. Along the boundaries  $x = L_x$  and  $z = L_z$ , we impose the free boundary condition. For the initial condition, we consider the static relativistic Harris current sheet (Hoh 1966; Kirk & Skjæraasen 2003):

$$B_z(x) = B_0 \tanh(x/\delta), \quad (3)$$

$$p(x) = p_{in} + p_s / \cosh^2(x/\delta), \quad (4)$$

$$\rho(x) = \rho_{in} + \rho_s / \cosh^2(x/\delta), \quad (5)$$

where  $p, \rho$  are the gas pressure and the rest mass density, and other variables are set to 0 except for a small perturbation of the magnetic field described later. For the upstream region of the current sheet, we consider a cold plasma  $\rho_{in} = 10p_{in}$ ; for the inside of the sheet, we consider a relativistically hot plasma  $\rho_s = p_s$  where  $p_s = B_0^2/8\pi$ . Note that the temperature of the sheet decreases with decreasing magnetic field strength.

<sup>1</sup> Note that in Fig. 3 of Sec. 4.2, we change the simulation box size  $L_z$  to explore the property of the magnetic reconnection rate over a large parameter space of the Lundquist number. In the other part, we set  $L_z = 320\delta$ .

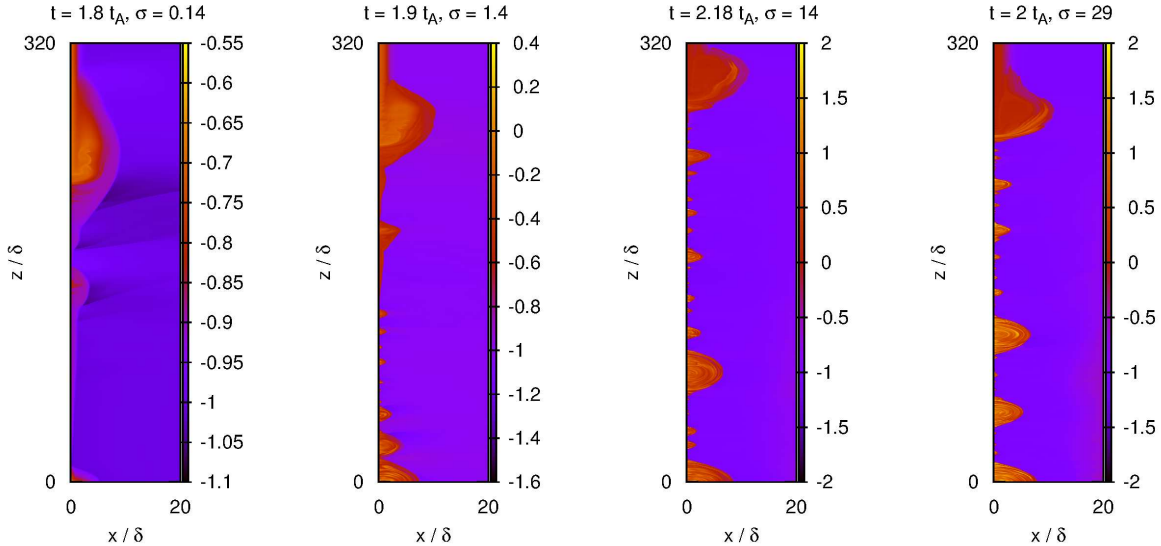


FIG. 1.— Snapshots of the temperature profile  $\log_{10}[k_B T/mc^2]$  of runs B1-B4 just before the largest plasmoid run away from the numerical domain where  $t_A = L_z/c_A$  is the Alfvén crossing time along the current sheet.

In this calculation, we use a constant resistivity  $\eta$  to concentrate on investigating the effect of the plasmoid-chain on the reconnection rate. Since it is easy to extend the law of resistivity, we will consider various kind of resistivity in our future work<sup>2</sup>. To trigger the initial tearing instability at the origin  $(x, z) = (0, 0)$ , we add the following small perturbation to the magnetic field:

$$\delta A_y = -0.03 B_0 \delta \exp[-(x^2 + z^2)/4\delta^2]. \quad (6)$$

Typical parameters used in our calculations are listed on Table 1. To model magnetic reconnection in high energy astrophysical phenomena, such as a relativistic jet, the Y-point of a pulsar magnetosphere and a gamma ray burst, we consider magnetically dominated plasma with magnetization parameter  $\sigma_{in} > 1$ . In the following sections, we present numerical results and consider the effects of the plasmoid-chain.

## 4. RESULTS AND DISCUSSION

In this section, we present numerical results of the tearing instability and evolution of the plasmoid-chain.

### 4.1. Temperature Profile

Fig. 1 shows snapshots of temperature profiles of runs B1-B4 at the time when the largest plasmoid to result from the initial perturbation reaches the edge of numerical domain. Since plasmoids move at approximately the Alfvén speed of the upstream flow unless the plasmoid inertia is comparable to the magnetic field energy, the escape time is of the order of  $t_A$ .

First, we find that many plasmoids evolve along the current sheet. As we mentioned in the previous section, the evolution of a plasmoid induces a thinner current sheet behind it, leading to a secondary tearing instability and the generation of a

the plasmoids-chain. We also find that the thickness of the current sheet between plasmoids decreases and the apparent number of plasmoids increases with increasing magnetization parameter  $\sigma$ . We will discuss this in Sec. 4.2. At the origin  $(x, z) = (0, 0)$ , we note the existence of a large hot region. This is an artifact of our assumption of point symmetry about the origin, which means that plasmoids entering the region from above have counterparts entering from below with the same magnitude and opposite speed. Their merger results in a plasmoid with zero momentum at the origin, which gradually accumulates matter as the simulation proceeds.

### 4.2. Reconnection Rate

Fig. 2 shows the time evolution of the reconnection rate in units of the Alfvén crossing time,  $L_z/c_A \equiv t_A$ . The reconnection rate is defined as:

$$v_R/c_A \equiv -\frac{c}{B_0 c_A L_z} \int_0^{L_z} dz E_y(x=0, z). \quad (7)$$

The top panel is the result of B3 plotted using a logarithmic scale. Here, we see that the evolution of the reconnection rate can be divided into three phases, separated in the figure by vertical lines at  $t = t_A$  and  $t = 2.2t_A$ . To the left of the blue line, the reconnection rate shows exponential growth due to the initial tearing instability at the origin. Between the blue and green lines, the reconnection rate oscillates around a power law growth rate with index approximately 2. This is the region where the plasmoid-chain develops: small plasmoids start to appear, changing the growth rate from exponential to power law<sup>3</sup>. Finally, the reconnection rate saturates to the right of the green line, which marks the time when the largest plasmoid escape.

In the bottom panel, we compare reconnection rates of runs B1-B4. We find that runs B2-B4 show very similar evolution after the plasmoid instability is triggered. This indicates that the reconnection rate in units of the Alfvén velocity,  $v_R/c_A$ ,

<sup>2</sup> In the case of a plasma with high temperature, the Coulomb collision cross section is usually very small and the collisional resistivity is also very small. However, if the plasma temperature rises up to the relativistic temperature  $k_B T \sim mc^2$  where  $k_B$  is the Boltzmann constant and  $m$  is the particle rest mass, the photon density in the plasma becomes very dense and the Compton drag becomes effective as a dominant collisional process (Goodman & Uzdensky 2008).

<sup>3</sup> This might be due to the self-similarity of structures in the plasmoid-chain (Shibata & Tanuma 2001; Uzdensky et al. 2010).

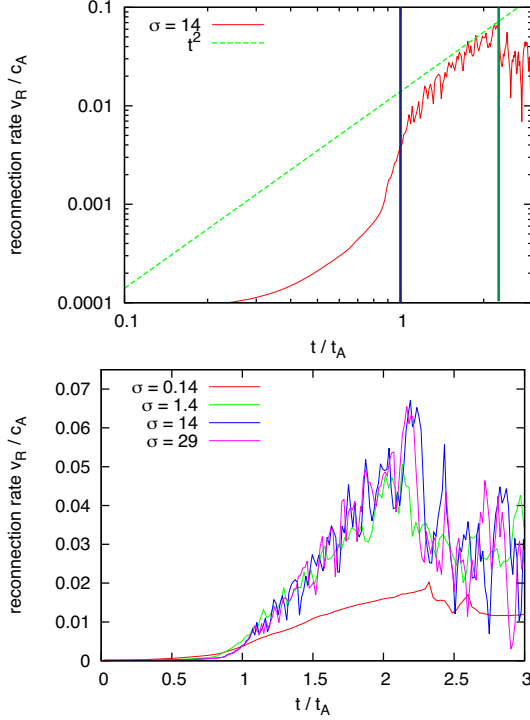


FIG. 2.— Top: The temporal evolution of the reconnection rate in the case of  $\sigma_{in} = 14$ . The blue line at  $t = t_A$  is the starting time of the plasmoid instability. The green line at  $t = 2.2t_A$  is the time when the largest plasmoid goes away from the numerical domain. Bottom: The temporal evolution of the reconnection rate of runs B1-B4.

becomes nearly independent of the magnetization parameter  $\sigma$  in the strongly magnetized plasma,  $\sigma_{in} > 1$ , once the plasmoid instability starts. The reconnection rate grows until the largest plasmoid, which is initially triggered at the origin, escapes from the numerical domain, at which point the reconnection rate has increased up to  $\sim 0.05c_A$ . After this, the plasmoid-chain reaches a statistical steady state and the averaged reconnection rate is about  $0.03c_A$ , which is approximately twice that of the relativistic tearing instability without a plasmoid-chain (Takahashi et al. 2011). Note that the reconnection rate of run B1 is lower than that of other runs. This is because in this case the plasmoid-chain does not grow sufficiently as can be seen in the left panel of Fig. 1 where only one secondary plasmoid is generated. This reduces its reconnection rate comparing with other runs including the fully evolved plasmoid-chain. We discuss later the reason why the plasmoid instability does not grow in this case.

Fig. 3 are the time-averaged reconnection rate  $\langle v_R/c_A \rangle$  as a function of the Lundquist number  $S_L$ <sup>4</sup>. The top panel is the relativistically strong magnetic field case,  $\sigma_{in} = 14$ , and the bottom panel is the non-relativistic magnetic field case,  $\sigma_{in} = 0.14$ . We calculate the time average of the reconnection rate curves over the plateau region where the plasmoid-chain reaches a statistical equilibrium state. As in the non-relativistic case, we find that the reconnection rate becomes independent of the Lundquist number when it is larger than a critical value  $S_c$ . For small Lundquist numbers, we find

<sup>4</sup> Our numerical code includes the following numerical dissipation,  $\eta_{num} \sim 0.03c\Delta$ , where  $\Delta$  is the mesh size. This means our numerical code can calculate accurately problems with the Lundquist number up to  $S_{num} = LC_A/\eta_{num} \sim 20Nc_A/c$  where  $N$  is the mesh number along the current sheet. As explained in Sec. 3, we use the mesh number  $N = 8192$  along the current sheet, our calculation has sufficient accuracy up to  $S_L \sim 3 \times 10^5$ .

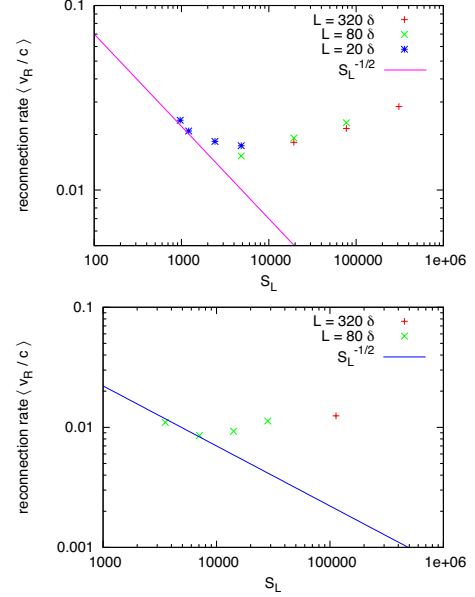


FIG. 3.— The plot of the time averaged reconnection rate  $\langle v_R/c_A \rangle$  over the statistical equilibrium region with respect to the Lundquist number  $S_L$ . Top: The strongly magnetized case:  $\sigma_{in} = 14$ . Bottom: The weakly magnetized case:  $\sigma_{in} = 0.14$ .

the Sweet-Parker sheet dependence  $S_L^{-1/2}$  of the reconnection rate predicted by Lyutikov & Uzdensky (2003) and Lyubarsky (2005) (see also Eq. (A11)). In our calculations, the critical value of the weakly magnetized case is  $S_c \sim 10^4$ , which is similar to the value indicated in the non-relativistic work; on the other hand, in the strongly magnetized case the critical value is  $S_c \sim 2-3 \times 10^3$ , which is a little less than that of the weak magnetic field case. This can be explained as follows. After generating plasmoids, the current sheet between the plasmoids will become a Sweet-Parker current sheet. In this case, the sheet thickness can be obtained by Eq. (A4). If we assume the reconnection jet velocity is the Alfvén velocity, the sheet thickness can be written as,  $\delta = L/\sqrt{2\sigma_{in}S_L}$ , where we used Eq. (A20) to estimate  $v_{in}$ . This means the sheet thickness decreases with increasing the magnetic field strength. On the other hand, the growth time of the tearing instability is,  $\sim \sqrt{\delta^3/\eta c_A}$ . Using these two expressions, the growth time of the tearing instability of the secondary current sheet is

$$\tau_{tearing,2nd} \sim \frac{\tau_{A,L}}{(2\sigma_{in})^{3/4} S_L^{1/4}} \propto \sigma_{in}^{-3/4} c_A^{-5/4}. \quad (8)$$

This means as the magnetic field strength becomes strong, the secondary tearing instability grows faster and the plasmoid instability occurs much easier, especially along the reconnection jet resulted from the initially triggered plasmoid. Similarly, using the characteristic wavelength of the tearing instability,  $\lambda_{tearing} \sim \delta[\delta c_A/\eta]^{1/4}$ , the characteristic wavelength of the secondary tearing instability can be obtained as:

$$\lambda_{tearing,2nd} \sim L/[(2\sigma_{in})^{5/8} S_L^{3/8}] \propto \sigma_{in}^{-5/8} c_A^{-3/8}. \quad (9)$$

This also indicates that the plasmoid instability evolves more easily as the background magnetization parameter becomes larger. Note that Eq. (9) means that a background plasma with larger magnetization parameter demands a smaller Lundquist number with respect to the sheet length for the plasmoid instability due to the smaller characteristic wavelength of the secondary tearing instability. This also supports the results shown in Fig. 3, which indicates that the critical Lundquist

number becomes smaller as the magnetization parameter of the background plasma becomes larger.

As pointed out by Uzdensky et al. (2010), the reconnection rate of the plasmoid-chain can be written as,  $v_R/c_A \sim 1/\sqrt{S_c}$ , using the relation of the Sweet-Parker sheet. If we use the above critical values,  $S_c = 3 \times 10^3$ , in the strongly magnetized case, the reconnection rate is  $\sim 0.02c_A$ , which agrees with the values indicated in the top panel of Fig. 2.

#### 4.3. Evolution of Plasmoid Structure

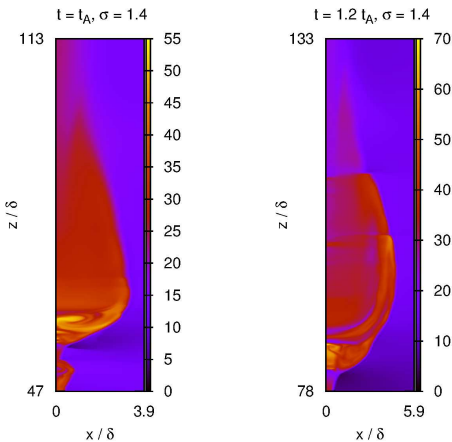


FIG. 4.— Snapshots of the density profile of the initially triggered plasmoid in the case of  $\sigma_{in} = 1.4$ . The left panel is at  $t = t_A$  and the right panel is at  $t = 1.2t_A$ .

Fig. 1 shows that the aspect ratio of plasmoids takes different values, depending on the magnetization parameter  $\sigma_{in}$ ; the aspect ratio seems to take a smaller value as the magnetization parameter  $\sigma_{in}$  increases. This can be explained as follows. Left panel of Fig. 4 is the density profile of a plasmoid at  $t = t_A$ . This figure shows its aspect ratio is about 14 : 1 and the inner structure of the plasmoid is very similar to that of the Petschek reconnection case which was investigated by Zenitani & Miyoshi (2011). Right panel of Fig. 4 is the density profile of the same plasmoid at  $t = 1.2t_A$ . We find that the plasmoid size in  $z$ -direction shrinks because of the appearance of slow shocks. These shocks are generated by the steepening of slow waves which are induced by collisions with other plasmoids. In the example shown in Fig. 4, slow waves are generated by the collision to the plasmoid at  $z \sim 48\delta$  in the left panel. As these slow shocks propagate across the plasmoid, the upstream plasma in the plasmoid is compressed and the plasmoid size shrinks in  $z$ -direction. Fig. 5 shows the density configuration of the plasmoid triggered by the initial perturbation of runs B1, B2 at a time just before it escapes from the numerical domain. In run B1,  $\sigma_{in} = 0.14$ , we find the aspect ratio of the plasmoid keeps its initial value, approximately 14 : 1. This is because in run B1 the plasmoid instability does not grow sufficiently as explained in the previous sections and the largest plasmoid does not experience a collision with a smaller plasmoid. On the other hand, in runs B2 many collision with smaller plasmoids reduce the aspect ratio of the plasmoids to about 6 : 1. In our calculations, the aspect ratio does not show any rapid time evolution after it

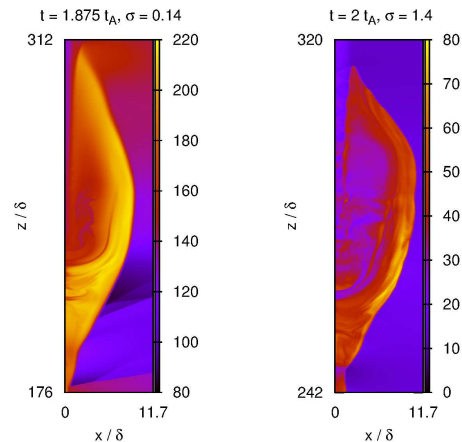


FIG. 5.— Snapshots of the density profile of the initially triggered plasmoid. The left panel is at  $t = 1.875t_A$  with weakly magnetized case,  $\sigma_{in} = 0.14$ , and the right panel is at  $t = 2t_A$  with strongly magnetized case,  $\sigma_{in} = 1.4$ .

reaches the above ratio, 6 : 1. Although we cannot be certain that this ratio is the final state, it seems that the aspect ratio depends very weakly on time. Finally, we cannot find any strong dependence of the above aspect ratio on the magnetization parameter  $\sigma$ .

#### 5. TRAJECTORY OF X AND O-POINTS

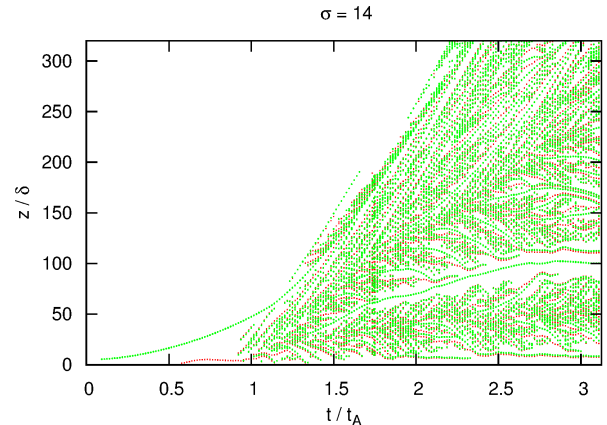


FIG. 6.— Trajectories of X and O points of the run B3 along the current sheet. Green points are the O-points and red points are the X-points.

To understand the physical nature of the plasmoid-chain, it is helpful to trace trajectories of the X and O points that are the magnetic null points:  $B_x = B_z = 0$ . At X-points, the magnetic configuration around them is the X-type and those are points where magnetic reconnection occurs; at O-points, the magnetic configuration around them is the O-type and they are usually equivalent to the location of a plasmoid. Fig. 6 is a plot of the trajectories of X and O points of run B3. This figure shows that in the initial phase there is only one O-point which is generated by the initial perturbation at the origin. Around  $t = t_A$ , small plasmoids start to develop behind the ini-

tial O-point and the number of O-points and X-points gradually increases with time. Around  $t = 2.2t_A$ , the initial plasmoid reaches the boundary of the numerical domain and escapes from the domain. After that, the current sheet is filled with X and O points, the plasmoid-chain is fully evolved. This is consistent with the temporal evolution of the reconnection rate shown in Fig. 2. Fig. 6 shows that most points, particularly those close to the initial plasmoid, move steadily towards larger  $z$ . Their velocity is approximately  $0.8c$ . Note that X and O points which are not close to the initial plasmoid gradually start to move in both directions along  $z$ -direction. This region is confined around the origin initially and expands with time as the plasmoid-chain evolves. Finally this region covers all the simulation domain and the plasmoid-chain reaches a statistical equilibrium state around  $t = 3t_A$ .

Concerning X-points, we find that they are located near the midpoint between two O-points as is expected since they are generated by the tearing instability which ejects two plasmoids away from the X-point. Fig. 6 shows that many X-points move along the current sheet and most of them disappear after a short time due to the merger of two neighboring plasmoids or the collapse of X-points (Loureiro et al. 2005). In addition, we find that X-points that move in a way similar to that of the nearest plasmoid as reported by Bárta et al. (2011b). Since X-points are considered to play an important role for the particle acceleration, their dynamical time along the current sheet will impose an upper limit on the acceleration time. For example, if we consider a current sheet with a plasmoid-chain in statistical equilibrium, with a critical Lundquist number  $S_c$ , the sheet length between them can be estimated as:  $L_c \sim S_c \eta / c_A$ ; the dynamical time can be estimated as

$$t_{acc} \sim L_c / c_A \sim S_c \eta / c_A^2, \quad (10)$$

and direct acceleration by the electric field at X-points will be limited by this time scale. Using our parameters, the value of the acceleration time is  $t_{acc} \sim 1.5 \times 10^{-2} t_A$ . Note that Fig. 6 includes X-points whose lifetime is much longer than the above value. Their typical lifetime is about  $1.5 \times 10^{-1} t_A$  and some of them survive for a much longer time. Fig. 6 indicates that they accompany large plasmoids which have somewhat large spaces around them.

Note that sometimes large spaces appear in the current sheet in Fig. 6, such as  $z = 0$  or  $z = 100\delta$ . This is due to the “*monster plasmoids*” which result from the merger of many smaller plasmoids. In particular, the monster plasmoid at  $z = 100\delta$  around  $t = 3t_A$  shows interesting behavior. In the initial phase, it behaves in nearly the same as other plasmoids. In the later phase, its inertia becomes much larger than that of surrounding plasmoids, and its dynamics starts to resemble Brownian motion, since it moves stochastically around an average trajectory that has a low velocity.

## 6. PLASMOID SIZE DISTRIBUTION

As mentioned in the previous sections, the evolution of a plasmoid induces a secondary tearing instability, and generates small plasmoids behind it; the small plasmoids in turn induce more tearing instabilities, and as a result the current sheet evolves into the plasmoid-chain. Since the distribution of plasmoid size is potentially important for high-energy astrophysical phenomena, we investigate this using our numerical results.

The statistical behavior of the plasmoid-chain was investigated in (Uzdensky et al. 2010; Fermo et al. 2010, 2011;

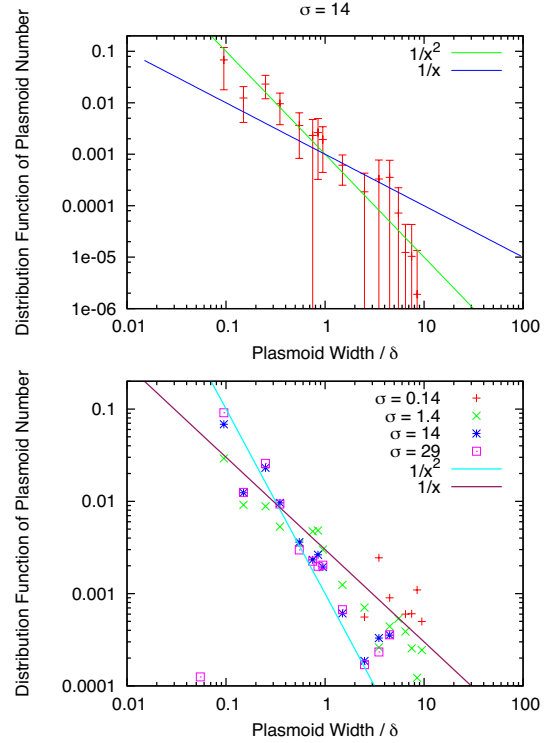


FIG. 7.— The time-averaged distribution function of plasmoid size perpendicular to the current sheet. The distribution functions are averaged over between  $t = t_A$  and  $t = 2.2t_A$ . Top: The distribution of run B3 with error bars. Bottom: The distributions of run B1-B4.

Loureiro et al. 2012; Huang & Bhattacharjee 2012, 2013). In those papers, the authors discuss the time evolution of the distribution function of the plasmoid-chain using the following model kinetic equation:

$$\frac{\partial f}{\partial t} + \alpha \frac{\partial f}{\partial \Psi} = \zeta \delta(\Psi) - \frac{fN}{\tau_A} - \frac{f}{\tau_A}, \quad (11)$$

where  $f(\Psi)$  is the distribution function,  $\Psi$  is the magnetic flux of a plasmoid,  $N(\Psi) \equiv \int_{\Psi}^{\infty} f(\Psi') d\Psi'$  is the cumulative distribution function,  $\alpha \sim B_0 c_A / \sqrt{S_c}$  is the plasmoid growing rate of a plasmoid,  $\tau_A \sim L / c_A$  is the Alfvén crossing time of a plasmoid across the plasmoid-chain with scale  $L$ , and  $\zeta$  is the magnitude of the source of plasmoids. Thus, the second term on the left-hand side describes the growth of plasmoids; the first term on the right-hand side is the source of plasmoids; the second term is the loss of plasmoids due to mergers with larger plasmoids; the third term is the advection loss. Some analytical steady state solutions of Eq. (11) in large  $\Psi$  region can be obtained as follows. When the loss of plasmoids is mainly by advection,  $N \ll 1$ , we obtain  $f \propto \exp[-\Psi / \alpha \tau_A]$ ; when the loss of plasmoids is mainly by plasmoid merger,  $N \gg 1$ , we obtain  $f \sim 2\alpha \tau_A \Psi^{-2}$ . In this derivation, we assumed the speed of plasmoids is of the order of  $c_A$ , corresponding to an assumption of the plasmoid crossing time as  $\tau_A \sim L / c_A$ . Recently, Huang & Bhattacharjee (2013) showed that dropping this assumption allows a solution  $f \propto \Psi^{-1}$ . Since the magnetic flux can be expressed as:  $\Psi \sim B_0 w$  where  $w$  is the plasmoid size perpendicular to their current sheet (Uzdensky et al. 2010), the above distribution function of the magnetic flux can be used to find the plasmoid size distribution.

The top panel of Fig. 7 is the time averaged distribution of the plasmoid size of run B3 with error bar. The time-

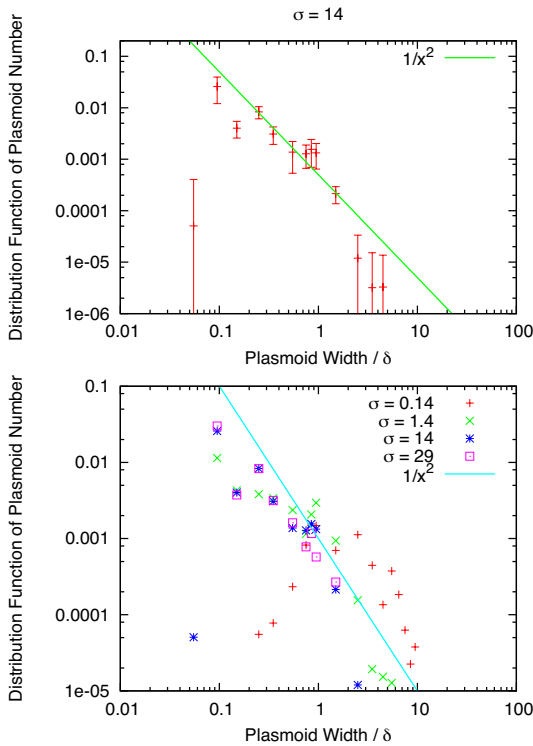


FIG. 8.— The time-averaged distribution of plasmoid size perpendicular to the current sheet. The distribution functions are averaged over after  $t = 2.2t_A$ . Top: The distribution of run B3 with error bars. Bottom: The distributions of run B1-B4.

average is taken over between  $t = t_A$  and  $t = 2.2t_A$  each of which is equivalent to the starting time of plasmoid instability and the escaping time of the initially triggered plasmoid, respectively, as indicated in Fig. 2 of Sec. 4.2. This figure shows that the plasmoid size distribution is consistent with a size distribution of power law index  $-2$  for small plasmoids in the range  $[0.1\delta, \delta]$  of the plasmoid width, as predicted by previous works for the non-relativistic case. From the above discussion, this means that the plasmoid loss is mainly due to plasmoid mergers. This is a natural consequence because we consider the distribution at the escape time of the initially triggered plasmoid and any plasmoids cannot escape from the plasmoid-chain at that time due to the presence of the initially triggered plasmoid. In addition, larger plasmoids, around  $\delta < w < 5\delta$ , deviate from the power law index  $-2$  and tend to an index of  $-1$ . This indicates that the velocity of large plasmoids deviates from the Alfvén velocity. This is because the large plasmoids have large inertia, which reduces their velocity, as in the case of the monster plasmoid. Note that the distribution function of the largest plasmoid size region, around  $w > 5\delta$ , drops rapidly and clearly deviates from power law. This is because the number of plasmoids is too small to show statistically sufficient results. This can also be seen from the large error bar of this region.

In the bottom panel of Fig. 7, we plot the plasmoid size distribution of runs B1-B4. We find that the distribution of the strong magnetic field case, run B4, shows very similar behavior to the run B3; it becomes a power law with index  $-2$  in the range  $[0.1\delta, \delta]$  of the plasmoid width and  $-1$  for larger plasmoids. In the weak magnetic field cases, runs B1, B2, the distribution also has an index of  $-1$  in the range of larger plasmoid. However, the distribution of the smaller plasmoid size region seems to have an index of  $-1$ , too. We consider this is

because small plasmoids are not sufficiently evolved in these runs to show a clear size dependence.

In Fig. 8, we plot the time-averaged distribution functions after the initially triggered plasmoids escaped:  $t > 2.2t_A$ . The top panel of Fig. 8 is the time averaged distribution of the plasmoid size of run B3 with error bar. In the small plasmoid region, the distribution function has an index of  $-2$ , similarly to the previous case. However, the distribution function of the larger plasmoid region,  $w > \delta$ , drops rapidly and clearly cannot be approximated by the power law. We consider this is due to the effect of the plasmoid loss by advection. Since the initially triggered plasmoid already escaped from the simulation domain in this case, the plasmoids can freely escape from the domain and this results in the exponential decay of the distribution function, as indicated by the above discussion using the kinetic equation.

The bottom panel of Fig. 8 is the plot of the plasmoid size distribution of runs B1-B4. The behavior of the distribution functions in small plasmoid region,  $w < \delta$ , is very similar to Fig. 7 but that in large plasmoid region also show rapid decay, similarly to the strongly magnetized case,  $\sigma = 14$ . Note that the distribution function of the weakly magnetized case,  $\sigma = 0.14$ , seems to be a power law in large plasmoid region,  $w > \delta$ . Unfortunately, our data does not have sufficiently large number of plasmoids in this region, so that we cannot conclude that this is a statistically correct result.

## 7. SUMMARY

In this paper, we investigated the evolution of the plasmoid-chain in a high- $\sigma$  plasma. We modeled the relativistic current sheet with cold background plasma using the relativistic resistive magnetohydrodynamic approximation, and solved its temporal evolution numerically. We performed various calculations using different magnetization parameters of the background plasma from  $\sigma_{in} = 0.14$  to  $\sigma_{in} = 29$  and different Lundquist numbers with respect to the sheet length from  $S_L \sim 10^3$  to  $S_L \sim 10^5$ . The numerical results show that the initially induced plasmoid triggers a secondary tearing instability and the current sheet is gradually filled with many plasmoids, that is, it evolves into a plasmoid-chain, as predicted by non-relativistic work. As expected, this plasmoid instability enhances the reconnection rate, which grows until the initially triggered plasmoid escapes from the simulation domain, reaching up to  $\sim 0.05c_A$ . Subsequently, the plasmoid-chain reaches a statistically equilibrium state, and the temporally averaged reconnection rate in a steady state becomes  $\sim 0.03c_A$ . Since the maximum value of the Alfvén velocity is the light velocity  $c$ , our numerical calculation indicates the maximum reconnection rate of the plasmoid-chain is  $0.03c$ . In our calculations, the evolution of the reconnection rate shows similar behavior in strongly magnetized cases:  $\sigma_{in} > 1$ . Although the weakly magnetized case,  $\sigma_{in} = 0.14$ , shows different behavior, we consider this is due to the larger wavelength of the secondary plasmoid instability indicated by Eq. (9). Note that the above critical value is much smaller than that obtained recently by Zanotti & Dumbser (2011), who found  $S_c \sim 10^8$ . We believe this difference comes from their assumption of a relativistically hot background plasma. A high temperature reduces the magnetization parameter  $\sigma_{in} = B_0^2/4\pi\rho_0 h_0 \gamma_0^2$  and the critical Lundquist number becomes large when  $\sigma$ -parameter is small, as shown in Sec. 4.2.

We also investigated the behavior of O-points and X-points. In our simulations, the initial perturbation is confined to the origin. The triggered plasmoid shrinks the current sheet be-

hind of it, inducing secondary tearing instabilities. Those O and X points that are close to the triggered plasmoid move in the same direction, but the other points start to move in both directions along the sheet, reflecting the final state of statistical equilibrium of the plasmoid-chain. Most X and O points disappear by merging, which limits their lifetime, and therefore, limits the time for which particles can be accelerated by the electric field at such points. We estimate this lifetime using the parameters of the plasmoid-chain. As predicted for the non-relativistic case, we noted the appearance of the “*monster plasmoids*”. Interestingly, our calculations show that “monster plasmoids” slow down as they evolve, because of their increasing inertia. Ultimately, they display Brownian like motion around fixed points.

Finally, we investigated the plasmoid size distribution. Our numerical results show that in strongly magnetized cases the distribution becomes power law with index  $-2$  in the small plasmoid region and  $-1$  in the large plasmoid region before the initially triggered plasmoid escapes. This indicates that the plasmoid loss is mainly due to mergers; the plasmoid velocity is of order of the Alfvén velocity in the small plasmoid region, but is lower in the large plasmoid region. This is because the plasmoid inertia increases with increasing size, preventing large plasmoids from moving at the Alfvén speed. After the escape of the initial plasmoid, the distribution function in large plasmoid region shows exponential decay because of the free advective escape of plasmoids from the domain.

Magnetic reconnection is one of the most efficient mechanisms of magnetic field dissipation, and is expected to play an important role in many astrophysical phenomena. As

shown in this paper, once the tearing instability evolves and generates plasmoids, the plasmoid-chain always evolves in the current sheet between them if the Lundquist number of the current sheets is beyond the critical value, especially in the Poynting-dominated plasma. Since plasmoids are associated with high temperature plasma and accelerated particles, they can be used to explain intermittent observational signals from high energy astrophysical objects, such as pulsed emission from the Y-point of the Crab pulsar magnetosphere (Uzdensky & Spitkovsky 2012) and multi-timescale TeV flares in blazars (Giannios 2013). In this paper, we assumed a constant resistivity and used an approximate equation of state corresponding to a relativistic, adiabatic gas. Nevertheless, we believe our results revealed general properties of plasmoid-chain in a Poynting dominant background plasma.

We would like to thank John Kirk, Iwona Mochol, Simone Giacche, Seiji Zenitani, Keizo Fujimoto, Takaaki Yokoyama and Tsuyoshi Inoue for many fruitful comments and discussions. We also would like to thank our referees for a lot of fruitful comments on our paper. Numerical computations were carried out on SR16000 at YITP in Kyoto University. Calculations were also carried out on the Cray XT4 at Center for Computational Astrophysics, CfCA, of National Astronomical Observatory of Japan. This work is supported by Max-Planck-Institut für Kernphysik and the Postdoctoral Fellowships for Research Abroad program by the Japan Society for the Promotion of Science No. 20130253 (M. T.).

## APPENDIX

### RELATIVISTIC SWEET-PARKER CURRENT SHEET

In this appendix, we derive the reconnection rate of the relativistic Sweet-Parker current sheet. The basic relations have already been presented by several authors (Blackman & Field 1994; Lyutikov & Uzdensky 2003; Lyubarsky 2005). Here, we clarify the dependence on the external pressure, following the non-relativistic approach of (Priest & Forbes 2000). A schematic picture of the Sweet-Parker current sheet is shown in Fig. A1.

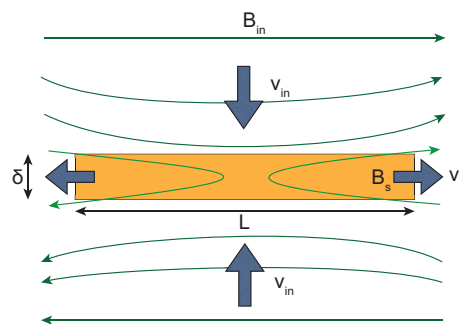


FIG. A1.— A schematic picture of the Sweet-Parker current sheet.

We assume a steady state plasma which can be described well by the relativistic magnetohydrodynamic approximation other than around the X-point. We also assume that the plasma is homogeneous in the  $y$ -direction. The background magnetic field of the inflow region is  $\mathbf{B}_{in} = B_{in}\mathbf{e}_x$  if  $z > \delta/2$  and  $\mathbf{B}_{in} = -B_{in}\mathbf{e}_x$  if  $z < -\delta/2$ , and that in the sheet region is  $\mathbf{B} = \epsilon\mathbf{B}_{in} \pm B_s\mathbf{e}_z$  where  $|B_{in}| \gg |B_s|$  and  $\epsilon$  is a very small constant. We assume that  $\mathbf{B} = \mathbf{0}$  at the X-point. In this case, the electric field  $E_y$  is constant, and we can obtain the following relation:

$$B_{in}v_{in} = B_s v_s, \quad (\text{A1})$$

where  $v$  is the fluid 3-velocity. In addition, we can obtain the following relation at the X-point where the magnetic field and flow velocity is 0:

$$B_{in}v_{in} = \eta j, \quad (\text{A2})$$



where  $\eta$  is the resistivity and  $j$  is the current vector described by the Ampère's law

$$j \sim B_{in}/\delta. \quad (A3)$$

From Eqs. (A2) and (A3), the sheet thickness  $\delta$  can be expressed as:

$$\delta \sim \eta/v_{in}. \quad (A4)$$

The mass and the energy conservation equation are given by

$$\rho_{in}\gamma_{in}v_{in}L = \rho_s\gamma_s v_s \delta, \quad (A5)$$

$$(\rho_{in}h_{in}\gamma_{in}^2 + B_{in}^2)v_{in}L = (\rho_s h_s \gamma_s^2 + B_s^2)v_s \delta, \quad (A6)$$

where  $\rho$  is the rest mass density,  $\gamma$  is the Lorentz factor,  $L$  is the curvature scale of the background magnetic field and  $\delta$  is the current sheet thickness.  $h = 1 + \Gamma/(\Gamma - 1)p/\rho$  is the specific enthalpy of the ideal gas where  $\Gamma = 4/3$  is the relativistic heat ratio and  $p$  is the gas pressure. Here, we also assume the cold upstream plasma,  $p_{in} = 0$ ; in the sheet region we assume a hot plasma  $\rho_s \ll \rho_s$  whose pressure can be determined through the pressure equilibrium,  $p_s = B_{in}^2/2\gamma_{in}^2$ . Then, the energy equation can be rewritten as

$$\rho_{in}\gamma_{in}^2(1 + \sigma_{in})v_{in}L = \left[ \frac{2B_{in}^2\gamma_s^2}{\gamma_{in}^2} + B_s^2 \right] v_s \delta, \quad (A7)$$

where  $\sigma \equiv B^2/\rho h \gamma^2$  is the magnetization parameter. Using Eqs. (A1), the above equation reduces to

$$(1 + \sigma_{in})\gamma_{in}^2 v_{in} = \left[ 2\sigma_{in}\gamma_s^2 + \frac{\sigma_{in}}{v_s^2}\gamma_{in}^2 v_{in}^2 \right] \frac{\delta}{L}. \quad (A8)$$

Using Eqs. (A4),

$$(1 + \sigma_{in})\gamma_{in}^2 v_{in}^2 \sim \left[ 2\gamma_s^2 v_s^2 + \gamma_{in}^2 v_{in}^2 \right] \frac{\sigma_{in}}{S_l v_s}, \quad (A9)$$

where  $S_l \equiv Lc/\eta$  is the Lundquist number using the light velocity as the characteristic velocity. From this equation, we can obtain the following relation between  $v_{in}$  and  $v_s$ :

$$\gamma_{in}v_{in} \sim \sqrt{\frac{2}{S_l v_s - c_A^2}} \gamma_s v_s c_A, \quad (A10)$$

where  $c_A \equiv \sqrt{\sigma/(1 + \sigma)}$  is the Alfvén velocity. If we consider a plasma with high-Lundquist number  $S_l \gg 1$ , the above equation reduces to

$$\gamma_{in}v_{in} \sim \sqrt{\frac{2}{S_l}} \gamma_s \sqrt{v_s} c_A. \quad (A11)$$

This equation shows that the inflow velocity, the reconnection rate, is inversely proportional to  $\sqrt{S_l}$ , which is the same conclusion as the non-relativistic Sweet-Parker current sheet model. To obtain an explicit solution of the upstream velocity, we have to add another equation to the above equations. Here, we consider the equation of motion along the x-direction. The relativistic hydrodynamical equation of motion in the current sheet is given by

$$\frac{\rho_s h_s \gamma_s^2 v_s^2}{L} \sim j B_s - \frac{p_o - p_N}{L} \sim \frac{B_{in}}{\delta} B_s - \frac{p_o - p_N}{L}, \quad (A12)$$

where we used Eq. (A3),  $p_o$  is pressure at the edge of the current sheet, and  $p_N \sim p_s$  is pressure at the X-point, respectively. Note that the scale  $L$  is a characteristic scale length in the above equation, and it should be the curvature scale of the background magnetic field. Using the pressure equilibrium, the above equation reduces to

$$2 \frac{B_{in}^2 \gamma_s^2 v_s^2}{\gamma_{in}^2 L} \sim \frac{B_{in}}{\delta} B_s - \frac{p_o - p_N}{L}, \quad (A13)$$

From the mass conservation equation Eq. (A5) and Eq. (A1), we can obtain the following relation

$$\frac{B_s}{\delta} = \frac{B_{in}}{L} \frac{\rho_s \gamma_s}{\rho_{in} \gamma_{in}}. \quad (A14)$$

Substitute this relation into Eq. (A13), we obtain

$$2 \frac{B_{in}^2 \gamma_s^2 v_s^2}{\gamma_{in}^2 L} \sim \frac{B_{in}^2}{L} \frac{\rho_s \gamma_s}{\rho_{in} \gamma_{in}} - \frac{p_o - p_N}{L}. \quad (A15)$$

This equation reduces to

$$\gamma_s^2 v_s^2 \sim \frac{\rho_s \gamma_s \gamma_{in}}{2\rho_{in}} - \frac{\gamma_{in}^2}{B_{in}^2} (p_o - p_N). \quad (A16)$$

From the mass conservation equation Eq. (A5) and Eq. (A4), we can obtain the following relation:

$$\frac{\rho_s \gamma_s}{\rho_{in}} \sim \frac{\gamma_{in} v_{in} L}{v_s \delta} \sim \frac{\gamma_{in} v_{in}^2}{v_s} S_L. \quad (\text{A17})$$

Using this equation, Eq. (A16) can be rewritten as follows:

$$\gamma_s \sim \gamma_A \sqrt{1 + \frac{1}{2} \left[ 1 - \frac{p_o}{p_N} \right]} \equiv \gamma_A \alpha, \quad (\text{A18})$$

where  $\gamma_A$  is the Lorentz factor of the Alfvén velocity in the upstream region and  $\alpha$  is the effect of the pressure gradient. Note that when  $p_o > 3p_N$ ,  $\alpha$  becomes imaginary number. This is because in this case the reconnection outflow is prevented by the pressure gradient force and this means the break down of the assumption of the steady state. Using this equation and Eq. (A11), we obtain the following form of the reconnection rate:

$$\gamma_{in} v_{in} / c_A \sim \sqrt{\frac{2}{S_L}} \sqrt{\gamma_A c_A \alpha \sqrt{\gamma_A^2 \alpha^2 - 1}}, \quad (\text{A19})$$

where  $S_L \equiv L c_A / \eta$  is the Lundquist number relating to the Alfvén velocity. When  $p_o = p_N$ , the above equation reduces to

$$\gamma_{in} v_{in} / c_A \sim \sqrt{\frac{2}{S_L}} \sqrt{\sigma_{in}}, \quad (\text{A20})$$

which is equivalent to the relation obtained in (Lytikov & Uzdensky 2003). When  $p_o = 0$ , or the reconnection outflow is ejected into very cold region, Eq. (A19) means the reconnection rate is enhanced due to the pressure gradient force. Finally, when  $p_o > p_N$ , which is, for example, the case where plasmoids are existed at the edge of the current sheet, Eq. (A19) means the reconnection rate is reduced by the pressure gradient force.

#### REFERENCES

- Amano, T., & Kirk, J. G. 2013, ArXiv e-prints  
 Barkov, M. V., & Baushev, A. N. 2011, *New A*, 16, 46  
 Bárta, M., Büchner, J., Karlický, M., & Kotř, P. 2011a, *ApJ*, 730, 47  
 Bárta, M., Büchner, J., Karlický, M., & Skála, J. 2011b, *ApJ*, 737, 24  
 Bessho, N., & Bhattacharjee, A. 2012, *ApJ*, 750, 129  
 Bhattacharjee, A., Huang, Y.-M., Yang, H., & Rogers, B. 2009, *Physics of Plasmas*, 16, 112102  
 Biskamp, D. 2000, *Magnetic Reconnection in Plasmas*, ed. Biskamp, D. Blackman, E. G., & Field, G. B. 1994, *Physical Review Letters*, 72, 494  
 Dumbser, M., & Zanotti, O. 2009, *Journal of Computational Physics*, 228, 6991  
 Evans, C. R., & Hawley, J. F. 1988, *ApJ*, 332, 659  
 Fermo, R. L., Drake, J. F., & Swisdak, M. 2010, *Physics of Plasmas*, 17, 010702  
 Fermo, R. L., Drake, J. F., Swisdak, M., & Hwang, K.-J. 2011, *Journal of Geophysical Research (Space Physics)*, 116, 9226  
 Fujimoto, K. 2011, *Physics of Plasmas*, 18, 111206  
 Furth, H. P., Killeen, J., & Rosenbluth, M. N. 1963, *Physics of Fluids*, 6, 459  
 Gardiner, T. A., & Stone, J. M. 2005, *Journal of Computational Physics*, 205, 509  
 —. 2008, *Journal of Computational Physics*, 227, 4123  
 Giannios, D. 2013, *MNRAS*, 431, 355  
 Goodman, J., & Uzdensky, D. 2008, *ApJ*, 688, 555  
 Hoh, F. C. 1966, *Physics of Fluids*, 9, 277  
 Huang, Y.-M., & Bhattacharjee, A. 2012, *Physical Review Letters*, 109, 265002  
 —. 2013, ArXiv e-prints  
 Inoue, T. 2012, *ApJ*, 760, 43  
 Kennel, C. F., & Coroniti, F. V. 1984a, *ApJ*, 283, 694  
 —. 1984b, *ApJ*, 283, 710  
 Kirk, J. G., & Skjærraasen, O. 2003, *ApJ*, 591, 366  
 Komissarov, S. S., Barkov, M., & Lyutikov, M. 2007a, *MNRAS*, 374, 415  
 Komissarov, S. S., Barkov, M. V., Vlahakis, N., & Königl, A. 2007b, *MNRAS*, 380, 51  
 Kowal, G., Lazarian, A., Vishniac, E. T., & Otmianowska-Mazur, K. 2009, *ApJ*, 700, 63  
 Lazarian, A., & Vishniac, E. T. 1999, *ApJ*, 517, 700  
 Loureiro, N. F., Cowley, S. C., Dorland, W. D., Haines, M. G., & Schekochihin, A. A. 2005, *Physical Review Letters*, 95, 235003  
 Loureiro, N. F., Samtaney, R., Schekochihin, A. A., & Uzdensky, D. A. 2012, *Physics of Plasmas*, 19, 042303  
 Loureiro, N. F., Schekochihin, A. A., & Cowley, S. C. 2007, *Physics of Plasmas*, 14, 100703  
 Loureiro, N. F., Schekochihin, A. A., & Uzdensky, D. A. 2013, *Phys. Rev. E*, 87, 013102  
 Lovelace, R. V. E., & Romanova, M. M. 2003, *ApJ*, 596, L159  
 Low, B. C. 1973, *ApJ*, 181, 209  
 Lyubarsky, Y., & Kirk, J. G. 2001, *ApJ*, 547, 437  
 Lyubarsky, Y. E. 2005, *MNRAS*, 358, 113  
 Lyutikov, M., & Blandford, R. 2003, ArXiv Astrophysics e-prints  
 Lyutikov, M., & Uzdensky, D. 2003, *ApJ*, 589, 893  
 Mochol, I., & Kirk, J. G. 2013a, ArXiv e-prints  
 —. 2013b, ArXiv e-prints  
 Parker, E. N. 1957, *J. Geophys. Res.*, 62, 509  
 —. 1963, *ApJS*, 8, 177  
 Priest, E., & Forbes, T. 2000, *Magnetic Reconnection*, ed. Priest, E. & Forbes, T.  
 Samtaney, R., Loureiro, N. F., Uzdensky, D. A., Schekochihin, A. A., & Cowley, S. C. 2009, *Physical Review Letters*, 103, 105004  
 Shibata, K., & Tanuma, S. 2001, *Earth, Planets, and Space*, 53, 473  
 Sweet, P. A. 1958, in *IAU Symposium, Vol. 6, Electromagnetic Phenomena in Cosmical Physics*, ed. B. Lehnert, 123  
 Takahashi, H. R., Kudoh, T., Masada, Y., & Matsumoto, J. 2011, *ApJ*, 739, L53  
 Takamoto, M., & Inoue, T. 2011, *ApJ*, 735, 113  
 Takamoto, M., Inoue, T., & Inutsuka, S.-i. 2012, *ApJ*, 755, 76  
 Ugai, M., & Zheng, L. 2005, *Physics of Plasmas*, 12, 092312  
 Uzdensky, D. A., Loureiro, N. F., & Schekochihin, A. A. 2010, *Physical Review Letters*, 105, 235002  
 Uzdensky, D. A., & Spitkovsky, A. 2012, ArXiv e-prints  
 Zanotti, O., & Dumbser, M. 2011, *MNRAS*, 418, 1004  
 Zenitani, S., Hesse, M., & Klimas, A. 2009a, *ApJ*, 705, 907  
 —. 2009b, *ApJ*, 696, 1385  
 —. 2010, *ApJ*, 716, L214  
 Zenitani, S., & Miyoshi, T. 2011, *Physics of Plasmas*, 18, 022105  
 Zhang, B., & Yan, H. 2011, *ApJ*, 726, 90